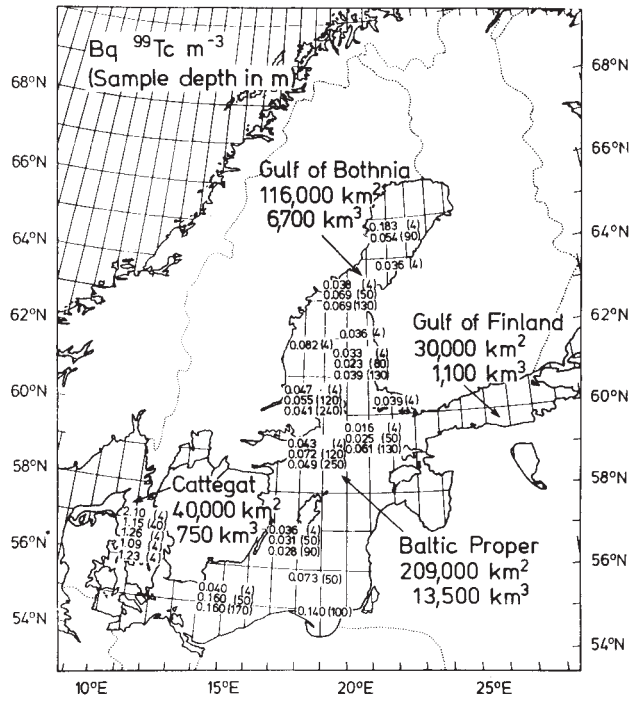

Fig. 1 Technetium concentrations in Baltic seawater collected in October–November 1986.

limit implies that ^{99}Tc/^{137}Cs was less than 5×10^{-4}, again consistent with the above.

Salo *et al.*[19] have calculated the global fallout inventories of ^{90}Sr and ^{137}Cs in the Baltic Sea. The calculated inventory in any year was obtained[20] by adding the contributions from direct deposition on the sea surface (precipitation), run-off (with rivers) and inflow through the Danish Straits, and subtracting the outflow through the Straits and the radioactive decay. If the subtraction of decay is omitted, we obtain the inventory that would pertain if the radionuclides (^{90}Sr or ^{137}Cs) had been stable and thus comparable with ^{99}Tc, which in practice behaved as a stable isotope during the period of observation. As the sedimentation and runoff characteristics of ^{99}Tc are closer to those of ^{90}Sr than to ^{137}Cs (refs 2, 21), we used the ^{90}Sr data. In 1981 Salo *et al.* estimated a ^{90}Sr inventory of 552 TBq; this corresponds to an undecayed amount of 811 TBq ^{90}Sr. According to UNSCEAR[22], the ^{137}Cs/^{90}Sr ratio in global fallout is 1.6; therefore, the ^{99}Tc/^{90}Sr ratio is 1.6 times the ^{99}Tc/^{137}Cs ratio in undecayed global fallout. Hence we estimate the inventory of global fallout-derived ^{99}Tc in the Baltic as 0.2 TBq.

The total inventory of ^{99}Tc in the Baltic Sea was calculated as follows. In the Gulf of Bothnia (comprising the Bothnian Bay and the Bothnian Sea) we assumed no halocline. Thus we used the mean of all eleven measurements, 0.060 Bq ^{99}Tc m^{-3}, multiplied by the water volume, 6,700 km^3 (ref. 19) giving an inventory of 0.40 TBq ^{99}Tc. In the Baltic Proper (see Fig. 1) and the Gulf of Finland there is a halocline at ~50 m depth. The water volumes above and below the halocline are 11,100 km^3 and 3,500 km^3 respectively. From Table 1 we calculated the mean of the eleven samples from the Baltic Proper with a sampling depth ≤50 m and of the eight samples collected below 50 m. These means, 0.050 and 0.076 Bq ^{99}Tc m^{-3} respectively, were multiplied by their respective volumes, giving 0.55 TBq ^{99}Tc above the halocline, 0.27 TBq below and a total inventory of 1.22 TBq ^{99}Tc. The latter is similar to the mean of all 30 samples (excluding those from the Cattegat) multiplied by the total volume, which gives 1.28 TBq ^{99}Tc. Our best estimate of the inventory is 1.3 TBq ^{99}Tc, and thus our estimate of the contribution from reprocessing is 1.05 TBq ^{99}Tc. As it takes 5–6 yr for discharges from Sellafield to enter the Baltic Proper[19], this amount of ^{99}Tc represents discharges up to 1980. Compared with the 0.6 PBq ^{99}Tc discharged from Sellafield from 1970 to 1980[3,23], the ^{99}Tc inventory in the Baltic Sea from reprocessing amounts to ~0.18% of the total release.

As the Baltic was the sea where maximum water concentration of ^{99}Tc was most likely to occur after the Chernobyl accident, and as we were unable to detect any additional ^{99}Tc in the Baltic sea water after the accident, we conclude that the Chernobyl accident did not contribute significantly to ^{99}Tc levels in the north-eastern Atlantic Ocean. Discharges from nuclear reprocessing in western Europe remain the dominant source of this radionuclide.

This project was supported by the CEC Radiation Protection Programme. Dr Chen had been awarded a fellowship under the International Atomic Energy Agency. We thank the F/S *Gauss* and its crew for hosting us during the cruise to the Baltic Sea.

Received 7 March; accepted 3 August 1988.

1. *ICRP Publication* **38** (Pergamon, Oxford-New York-Frankfurt, 1983).
2. Aarkrog, A. *et al. Estuar. Coast. Shelf Sci.* **24,** 637–647 (1987).
3. Jefferies, D. F., Steele, A. K. & Preston, A. *Deep Sea Res.* **29,** 713–738 (1982).
4. Kautsky, H. *Dt. hydrogr. Z.* **40,** 49–69 (1987).
5. Livingston, H. D., Bowen, V. T. & Kupferman, S. L. *J. mar. Res.* **40,** 1227–1258 (1982).
6. Devell, L., Aarkrog, A., Blomqvist, L., Magnusson, S. & Tveten, U. *Nuclear Europe* **VI,** 16–17 (1986).
7. *Tech. Rep. Ser. 247: Sediment K_ds and Concentration Factors for Radionuclides in the Marine Environment* (Int. Atomic Energy Agency, Vienna, 1985).
8. Holm, E., Rioseco, J. & Mattsson, S. in *Technetium in the Environment* (eds Desmet, G. & Myttenaere, C.) 61–68 (Elsevier, 1984).
9. *Meereskudliche Beobachtungen und Ergebnisse Nr 62* (Deutsches Hydrographisches Institut, Hamburg, 1987).
10. Buesseler, K. O. *et al. Nature* **329,** 825–828 (1987).
11. Holm, E., Rioseco, J. & Garcia-Leon, M. *Nucl. Instrum. Meth. Phys. Res.* **223,** 204–207 (1984).
12. Chen, Q., Aarkrog, A., Dick, H. & Mandrup, K. *Risø-M-2671* (Risø National Laboratory, 1987).
13. Aarkrog, A. *et al. Risø-R-540* (Risø National Laboratory, 1987).
14. Harley, J. H. *HASL-300* (Environmental Measurements Laboratory, New York, 1972).
15. Till, J. E. in *Technetium in the Environment* (eds Desmet, G. & Myttenaere, C.) 1–20 (Elsevier, 1984).
16. *Summary Report on the Post-Accident Review Meeting on the Chernobyl Accident* Safety Series No 75-INSAG-1 (IAEA, Vienna, 1986).
17. ApSimon, H. M., Macdonald, H. F. & Wilson, J. J. N. *J. Soc. radiol. Prot.* **6,** 109–119 (1986).
18. *Environmental Health Series No 24: Health Hazards from Radiocaesium Following the Chernobyl Nuclear Accident* (World Health Organization, Copenhagen, 1987).
19. *Study of Radioactive Materials in the Baltic Sea* IAEA-TEC-DOC-362 (Int. Atomic Energy Agency, Vienna, 1986).
20. Salo, A. & Voipio, A. *Mar. Pollution Bull.* **12,** 218–224 (1981).
21. Blaylock, B. G., Frank, M. L., Hoffman, F. O. & De Angelis, D. L. in *Technetium in the Environment* (eds Desmet, G. & Myttenaere, C.) 79–89 (Elsevier, 1984).
22. *UNSCEAR, Ionizing Radiation: Sources and Biological Effects* (United Nations, New York, 1982).
23. *BNFL Annual Reports on Radioactive Discharges and Monitoring of the Environment* (British Nucl. Fuels Ltd, Risley, 1978–85).

Seismological and structural evolution of strike-slip faults

Steven G. Wesnousky

Center for Earthquake Research and Information,
Memphis State University, Memphis, Tennessee 38152, USA

The mapped traces of strike-slip faults are commonly characterized by discontinuities that appear as steps in map-view. Here I present observations to show that the number of steps per unit length along the trace of major strike-slip fault zones in California and Turkey is a smoothly decreasing function of cumulative geological offset. When coupled with a growing body of evidence that indicates that steps in fault traces work to impede or arrest the propagation of earthquake ruptures, the apparent smoothing of fault traces with displacement is interpreted to suggest that the spatial distribution of strength properties on a fault plane is a function of cumulative geological offset. A consequence of this structural evolution is that faults may undergo a seismological evolution a well, whereby the size and frequency distribution of earthquakes is also a function of cumulative offset.

An earthquake in California or other region of similar tectonic style does not generally rupture the whole length of the fault

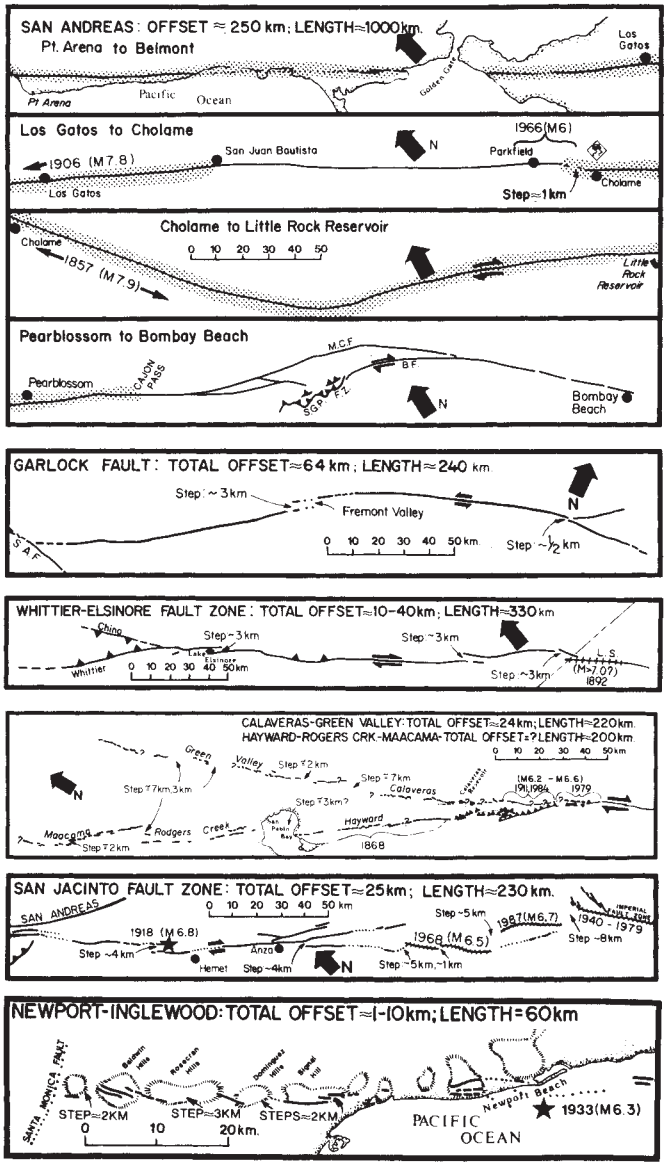

Fig. 1 Maps of the San Andreas[16-22], Garlock[23], Whittier-Elsinore[24], Calaveras-Green Valley[25], San Jacinto[26] and Newport-Inglewood[13] fault zones of California showing the location of steps in fault traces which are characterized by stepover widths $W_s \geq$ 1 km. Segments of fault which have ruptured during historical earthquakes are marked by hachures, stippling or brackets, and the dates and magnitudes of the respective earthquakes. Epicentre of 1933 Long Beach earthquake is marked by star and half-sided arrows indicate sense of displacement along faults.

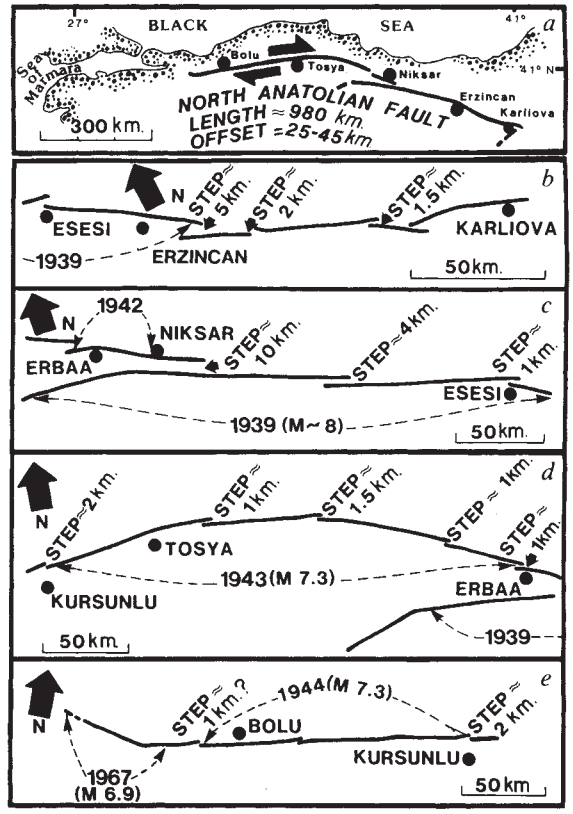

Fig. 2 *a*, The North Anatolian fault shows right-lateral movement and strikes westward across Turkey from a point near Karliova to west of Bolu. Larger-scale and overlapping strip maps of the fault (*b–e*) are taken from Barka and Kadinsky-Case[5] and show location of steps greater than about 1 km in size. Dates and arrows show the year and extent of rupture during large historical earthquakes, respectively.

on which it occurs but, rather, only a fraction of the entire fault length[1]. Observations also show that the endpoints of strike-slip earthquake ruptures are commonly associated with step-like discontinuities along mapped fault traces[2,3]. When slip occurs along a fault during an earthquake, stress concentrations will occur at step-like discontinuities along the fault[2]. Such discontinuities are commonly referred to as releasing- or restraining-steps, depending on whether the stress concentration is extensional or compressional in nature[4], respectively, and the severity of the stress concentration will generally be a function of the width W_s of the step as measured perpendicular to fault strike[2]. The stress concentrations at steps may be sufficient to impede or stop the propagation of an earthquake rupture and, on that basis, a number of investigators have attributed a causal association to the observed coincidence between the endpoints of earthquake ruptures and the location of steps along mapped fault traces[3,5]. In turn, laboratory models and scattered field observations have been the basis to suggest that, during the initial stages of development, strike-slip faults are characterized by a zone of discrete fault segments, each of which is separated from the next segment by a step, and that, with continued displacement, the individual fault segments ultimately coalesce to accommodate displacements along a principal and through-going fault[6,7]. The few observations available thus point to a close connection between the seismological and the structural evolution of fault zones and provided the impetus for this work: to examine whether or not there exists a systematic relationship between frequency of occurrence of step-like discontinuities and the total geological offset registered along the trace of active strike-slip faults.

Strike-slip fault zones and earthquakes in California and Turkey are the principal basis for my observations. It is for these regions that the most comprehensive maps and data concerning the total geological offset and the location of historical earthquakes along the trace of active faults are available. More specifically, I have relied on the published literature to obtain estimates of the cumulative geological offset across the San Andreas[8], Garlock[9], Whittier-Elsinore[10], Calaveras-Green Valley[11], San Jacinto[12] and Newport-Inglewood[13] faults of California and the North Anatolian fault zone[14] of Turkey. Similarly, the magnitude and rupture length of historical ruptures along strike of each of the fault zones has been the source of numerous previous studies[1,5]. Thus, the location and magnitude of historical earthquake ruptures, the total fault length, the cumulative geological offset and the locations and sizes of step-like discontinuities along strike of each of the fault zones considered have been detailed in a separate report[15] and are summarized in the accompanying maps (Figs 1 and 2). Because of the scale of

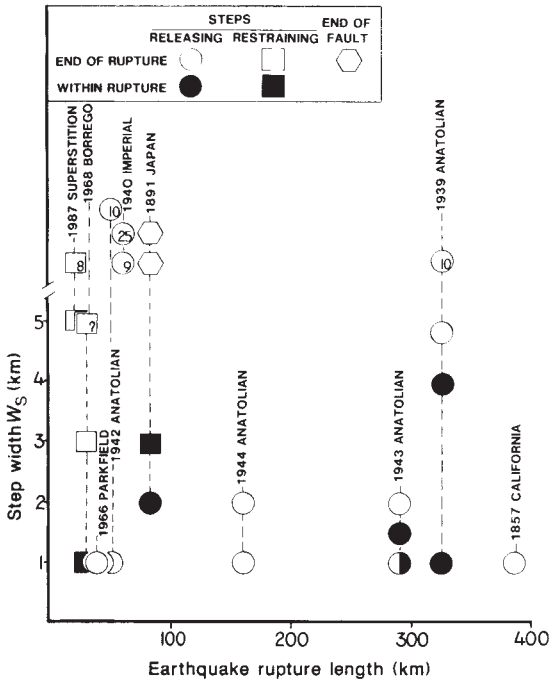

Fig. 3 Earthquake rupture length versus the size W_s of steps in mapped fault trace observed at the endpoints (open symbols) and within (solid symbols) the rupture zone of large Anatolian and California earthquakes. Half-filled symbol indicates that steps of similar size occurred both within and at endpoint of rupture. Steps in fault trace are also subdivided according to whether they are restraining (squares) or releasing (circles) in nature.

available maps, I have limited attention to steps in fault trace characterized by stepover widths of a kilometre or greater.

Figure 3 illustrates the relationship of the size and location of steps along the traces of strike-slip faults to the length and location of earthquake ruptures. The figure is a plot of the rupture lengths of large California and Anatolian earthquakes versus the stepover width W_s for each step in the fault trace observed at both the endpoints and within the respective earthquake rupture zones. For example, Fig. 3 shows that the 1939 Anatolian earthquake produced ~320 km of surface rupture and that the endpoints of the rupture are associated with steps of about 5 and 10 km respectively. The figure also shows that the same rupture propagated through steps of 1 and 4 km; that is to say, the steps located within the 1939 rupture zone are smaller than the steps associated with the termination of the rupture. A similar pattern is found for the other earthquakes in Fig. 3, that is, steps associated with the endpoints of ruptures are commonly the largest discontinuities registered along the length of the respective rupture zones. The trend, admittedly, is not without exception. The 1943 Anatolian earthquake is a case in point, where a step interior to the rupture zone is larger than a similar step observed at the endpoint of the rupture. It is also apparent that the endpoints of all ruptures are not marked by steps in mapped fault traces, as evidenced by the southern limit of the 1857 California earthquake (Fig. 1). Nonetheless, the observations are certainly sufficient to argue that the association of steps with the endpoints of earthquakes is not merely coincidence. Rather, the stress concentrations resulting from the discontinuities appear to play a principal and causal role in limiting the extent of earthquake ruptures.

A number of recent studies have attempted to explain characteristics of the spatial, temporal and size distributions of earthquakes along faults by assuming an arbitrary or fractal distribution of strength properties along fault planes[27-31]. The observations I have summarized thus far suggest that the

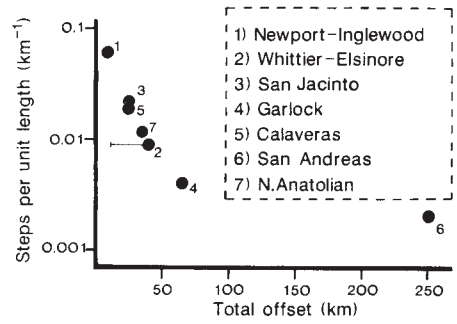

Fig. 4 The number of steps ($W_s \geq 1$ km) per unit length of mapped fault trace versus cumulative geological offset along major strike-slips faults in California and Turkey.

geometrical complexity of fault traces may be used to gauge, in a general sense, the heterogeneity of strength properties along fault planes. Toward that end, the number of steps ($W_s \geq 1$ km) per unit length of a fault zone provides a simple, quantitative measure of fault trace complexity. The complexity of fault trace measured in this manner is plotted as a function of cumulative geological offset in Fig. 4. Fault trace complexity varies by nearly two orders of magnitude within the data set and is a smoothly decreasing function of cumulative geological offset. The observation supports the idea that fault zones are characterized by a discontinuous trace during the initial stages of development and that increasing displacement along such faults works to remove discontinuities along the fault trace, effectively smoothing the fault plane. Moreover, when coupled with the growing body of evidence that indicates that steps in fault traces work to impede or arrest the propagation of earthquake ruptures, the apparent smoothing of the fault trace with displacement may be further interpreted to indicate that the distribution of strength properties on a fault plane is spatially heterogenous, and that the degree of heterogeneity is a function of cumulative offset. A consequence of this structural evolution is that faults may undergo a seismological evolution as well, whereby the size and frequency distribution of earthquakes on a fault is also a function of cumulative geological offset.

I thank A. Barka and A. Johnston for reviews of the manuscript, A. Barka, T. Rockwell and D. Herd for preprints of unpublished papers and maps, Tanya George for drafting the figures and the NSF for supporting the research.

Received 26 May; accepted 12 August 1988.

1. Wesnousky, S. G. *J. geophys. Res.* **91,** 12587-12631 (1986).
2. Segall, P. & Pollard, D. D. *J. geophys. Res.* **85,** 4337-4350 (1980).
3. Sibson, R. H. *Geophys. Monogr.* **37,** 157-167 (Am. Geophys. Un., Washington D.C., 1986).
4. Crowell, J. C. *Soc. econ. Paleontologists and Mineralogists spec. Pap.* **22,** 190-204 (1974).
5. Barka, A. A. & Kadinsky-Cade, C. *Tectonics* (in the press).
6. Wilcox, R. E., Harding, T. P. & Seely, D. R. *Bull. Am. Ass. Petrol. Geol.* **57,** 74-94 (1973).
7. Withjack, M. O. & Jamison, W. R. *Tectonophysics* **126,** 99-124 (1986).
8. Hill, M. L. *Geol. Soc. Am. Bull.* **92,** 112-131 (1981).
9. Smith, G. I. *Bull. Am. Assoc. Petrol. Geol.* **46,** 185-104 (1962).
10. Lamar, D. L. & Rockwell, T. K. in *Neotectonics and Faulting in Southern California, Guidebook and Volume* 82nd Annual Meeting of the Cordilleran Section of the Geol. Soc. Am. 149-158 (Los Angeles, California, 1986).
11. Kintzer, F. C., Brooks, E. R. & Cummings, J. C. *Geol. Soc. Am.* Abstracts with Programs **9,** 65 (1977).
12. Sharp, R. V. *Geol. Soc. Am. Bull.* **78,** 705-730 (1967).
13. Barrows, A. G. *Spec. Rep. Calif. Div. Mines Geol.* **114,** 115 (1974).
14. Barka, A. A. & Gulen, L. *Spec. Publs Middle East. tech. Univ.* (in the press).
15. Wesnousky, S. G. *Proc. USGS Workshop on Fault Segmentation and Controls of Rupture Initiation and Termination - USGS Open-File Report* (in the press).
16. Clark, M. M. *USGS Misc. Field Invest. Map.* **I-1483** (1984).
17. Hope, R. A. *USGS Open-file Rep.* **69-130** (1969).
18. Ross, D. C. *USGS Misc. Field Invest. Map* **I-553,** (1969).
19. Vedder, J. G. & Wallace, R. E. *USGS Misc. geol. Invest. Map* **I-574** (1970).
20. Brown, R. D. *USGS Misc. geol. Invest. Map* **I-575** (1970).
21. Brown, R. D. Jr & Wolfe, E. W. *USGS Misc. geol. Invest. Map* **I-692** (1972).
22. Matti, J. C., Morton, D. M. & Cox, B. F. *USGS Open-file Rep.* **85-365,** 23 (1985).
23. Clark, M. M. *USGS Misc. geol. Invest. Map* **74,** (1973).
24. Anderson, J. G., Rockwell, T. & Agnew, D. *Earthquake Spectra* (in the press).
25. Herd, D. G. *USGS Misc. Field Stud.* 1:250,000 *Map of Recently Active Faults of San Francisco Bay Region and Surrounding Northern California Coast Ranges* (in the press).
26. Sharp, R. V. *Bull. Calif. Div. Mines Geol.* **196,** 187-194 (1975).

27. Lay, T. & Kanamori, H. in *Earthquake Prediction: an International Review* (eds Simpson, D. & Richards, P.) 579-592 (Maurice Ewing Series 4, Am. Geophys. Un., Washington, D.C., 1981).
28. Andrews, D. J. *J. geophys. Res.* **85**, 3867-3877 (1980).
29. Aki, K. in *Earthquake Prediction - An International Review* (eds Simpson, D. & Richards, P.) 566-574 (Maurice Ewing Series 4, A. Geophys. Un., Washington, D.C., 1981).
30. Scholz, C. H. & Aviles, C. A. in *Earthquakes Source Mechanics* Geophys. Monogr. **37**, 147-156 (eds Das, S., Boatwright, J. & Scholz, C.) (Maurice Ewing Series 6, Am. Geophys. Un., Washington, D.C., 1986).
31. Smalley, R., Turcotte, D. & Solla, S. *J. geophys. Res.* **90**, 1894-1900 (1985).

An experimental determination of primary carbonatite magma composition

Margaret E. Wallace & David H. Green

Geology Department, University of Tasmania, GPO Box 252C, Hobart, Australia 7001

Carbonatites are uncommon carbonate-rich rocks usually found in continental intra-plate regions and often associated with rifting. There has been much debate as to whether carbonatite magmas are primary melts derived from partial melting of mantle peridotite, or are formed by exsolution of an immiscible carbonate melt fraction from phonolitic or nephelinitic magmas. Our experiments on the phase relationships of carbonate and amphibole-bearing peridotite (containing 0.3% H_2O and 0.5–2.5% CO_2) show that sodic dolomitic carbonatite magma coexists with an amphibole lherzolite assemblage in a field ranging from 21 to 30 kbar and 930 to 1,080 °C, spanning a pressure and temperature interval between the solidus and the amphibole breakdown and melting curve. Thus primary carbonatite melts may occur under suitable geothermal conditions. The nature of the peridotite solidus and of the melting reactions differ considerably from published models[1–3]. The carbonatite melt composition, determined by a series of 'sandwich' experiments, was found to be rich in Na, Mg, Ca and Fe, with a small dissolved silicate content. This melt quenches to an assemblage of dolomite and Na–Mg carbonate minerals, producing textures similar to those preserved in samples from Oldoinyo Lengai[4], Homa mountains, Tanzania[5] and Kaiserstuhl, Germany[6].

The majority of carbonites are rich in calcium and are composed of calcite (the calcite carbonatites, sövite and alvikite) and dolomite (beforsites or dolomite carbonatites) with minor amounts of ferroan carbonate. Cation abundance is in the order Ca > Mg > Fe > (Na + K) (ref. 7). These minerals characteristically contain high contents of Sr, Ba, Nb and rare earth elements, and are associated with ijolites and other alkali-rich igneous rocks, and commonly are surrounded by large sodic or potassic fenitization halos. A particularly important type of carbonatite has been erupted by Oldoinyo Lengai, northern Tanzania[4]. It is highly alkalic (Table 1, column 12) and is composed dominantly of Na_2O, K_2O, CaO and CO_2, which form the mixed carbonate minerals nyerereite $(Na_{0.22}K_{0.18})_2Ca(CO_3)_2$ and gregoryite $(Na_{0.78}K_{0.05})_2Ca_{0.17}CO_3$ (ref. 8). Several other carbonatite lavas, now composed largely of calcite, have been interpreted recently as originally having had similar mineralogy[9], subsequently replaced by reaction with calcium-rich ground water[4,5,9]. It is thus argued that alkali-rich carbonatite magma occurred more frequently than is indicated by the present relative abundance of calcitic carbonatites and natro-carbonatites.

Isotope studies demonstrate that carbonatitic magmas are derived from mantle source areas[10–12], but do not distinguish between origins by partial melting of the mantle or by exsolution from a phonolitic or nephelinitic magma[7,13–18]. Experimental investigations of carbonatite genesis have explored the CaO–MgO–SiO_2–CO_2–H_2O system, its subsystems and other systems involving alkali elements with CO_2 and H_2O[14,19–21]. This extensive literature has been summarized by Wyllie[22] and Eggler[23].

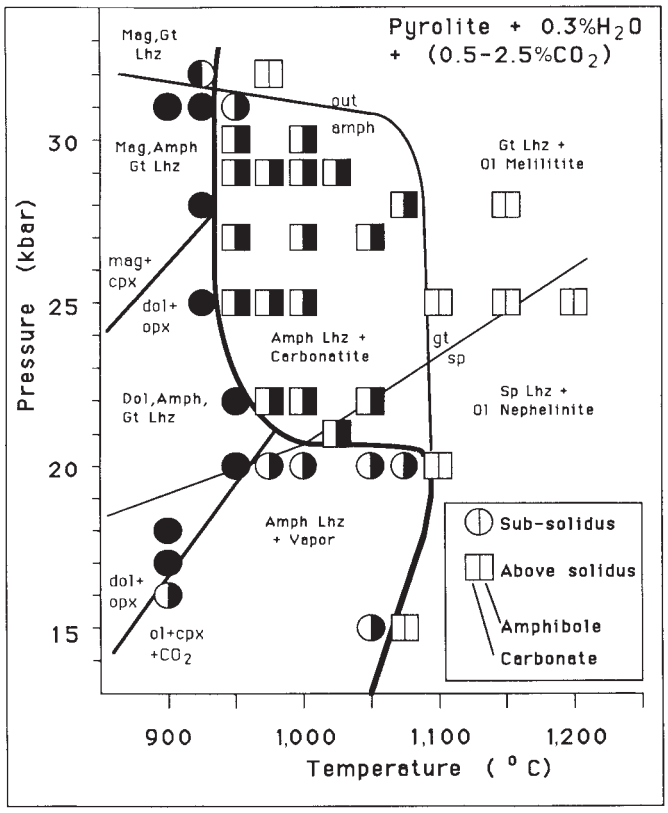

Fig. 1 Phase relationships of amphibole-rich Hawaiian Pyrolite (0.3% H_2O) plus 5% dolomite or 1.4% magnesite. Carbonatite melt field is bounded by the carbonate solidus at 930 °C (heavy line) and amphibole breakdown and silicate melt field above 1,080 °C (25 kbar). Size of the box symbols indicates the uncertainty in pressure and temperature. All runs were buffered with magnesite ($f_{O_2} \approx$ EMOG).

These earlier studies confirmed the existence of low-temperature alkali-rich carbonate melts, explored liquid immiscibility between silicate and carbonate-rich melts, and documented stability fields for carbonated peridotite under upper-mantle conditions. Other studies have investigated the solubility of CO_2 as (CO_3^{2-}) in silicate melts at high pressure[24–25] and have emphasized continuity at high pressures between kimberlite, olivine melilitite and carbonatite magma compositions. Although there is thus a generally accepted framework for carbonatite genesis in the upper mantle, there is a continuing debate on the relative importance of crystal fractionation (for example, to yield Oldoinyo Lengai natrocarbonatite magma as a differentiate from parental calcitic or dolomitic carbonatite[17]) and liquid immiscibility (for example, to yield Oldoinyo Lengai natrocarbonatite magma as an exsolution from parental carbonated nephelinite or phonolite magma[18]). The specific problem of accurate determination of both the solidus temperature of a carbonate-bearing lherzolite and the nature of the melt at the solidus at high pressures has frustrated experimental petrologists and generated much debate[1–3,22–27]. We have clarified the position of the peridotite solidus and we demonstrate that, because of the importance of the minor components Na, K, P and Ti, primary mantle melts of sodic, dolomitic carbonatite character can be produced under oxidizing conditions from amphibole and carbonate-bearing lherzolite.

Phase relationships for (amphibole pyrolite minus 40% olivine[27] plus 1.4% $MgCO_3$ or 5% $CaMgCO_3$) are presented in Fig. 1. The (amphibole pyrolite minus 40% olivine) starting-mix was prepared in 100-mg batches[27] and all phases analysed by microprobe. The peridotite composition used represents a vapour-undersaturated 'fertile' mantle peridotite, in which par-